Characterization and Spatial Source Apportionments of Ambient PM$_{10}$ and PM$_{2.5}$ during the Heating Period in Tian'jin, China

Baoshuang Liu[1], Xiaoyun Sun[1], Jiaying Zhang[1], Xiaohui Bi[1]*, Yafei Li[1], Liwei Li[2], Haiyan Dong[2], Zhimei Xiao[2], Yufen Zhang[1], Yinchang Feng[1]

[1] *State Environmental Protection Key Laboratory of Urban Ambient Air Particulate Matter Pollution Prevention and Control and Center for Urban Transport Emission Research, College of Environmental Science and Engineering, Nankai University, Tian'jin 300350, China*
[2] *Tianjin Eco-Environment Monitoring Center, Tian'jin 300071, China*

ABSTRACT

We collected ambient PM$_{10}$ and PM$_{2.5}$ samples from six sites in Tian'jin, China, from February to March 2016 and then analyzed their chemical compositions and identified the emission sources using the positive matrix factorization model. The mean concentrations of the PM$_{10}$ and PM$_{2.5}$ were 98 and 71 µg m^{-3}, respectively, with a mean PM$_{2.5}$/PM$_{10}$ ratio of 0.67. The average concentrations of the combined SO$_4^{2-}$, NO$_3^-$, and NH$_4^+$ were 19.9–23.4 µg m^{-3}, accounting for 72.4–77.1% of the total measured ions. The concentrations and percentages were significantly higher for NO$_3^-$ and OC than for other species. The SO$_4^{2-}$/NO$_3^-$ ratio showed a decreasing tendency as the PM$_{10}$ and PM$_{2.5}$ concentrations increased, implying a strong influence from mobile sources. The mean OC/EC ratios for PM$_{10}$ and PM$_{2.5}$ were 3.1 and 3.2, respectively, with small spatial differences. The most abundant elements were crustal, accounting for 73.2–84.2% of the total detected elemental mass, and mainly enriched in the PM$_{10}$. The optimal number of factors for PM$_{2.5}$ and PM$_{10}$ was selected via PMF analysis: the decrease in the Q/Q_{except} values of these two fractions lessened when choosing six instead of five factors, indicating that five factors may be optimal. All the factors were mapped in bootstrap (BS) for 100% of the runs, and no swaps occurred with the displacement of factor elements (DISP) for five factors. Secondary inorganic aerosol, coal combustion, crustal dust, vehicle exhaust, and biomass burning contributed 28–30%, 20–21%, 18–21%, 17–20%, and 4%, respectively. Secondary inorganic aerosol displayed less spatial heterogeneity than the other sources in its contributions. Backward trajectory and PSCF analysis showed that air masses affecting Tian'jin mainly originated in the northwest during the heating period, and northeastern He'nan, southwestern Shan'dong, Bei'jing, and Tian'jin itself were major potential source areas.

Keywords: Chemical species; Source apportionment; Heating period; Error estimation; PMF.

INTRODUCTION

Particulate matter (PM) is mainly composed of inorganic, carbonaceous, and elemental matter (Zhang *et al.*, 2013, 2014; Liu *et al.*, 2016a). Understanding PM chemical composition and source is critical to assessing impacts on air quality, climate change and human health, as well as to controlling pollution (Zhang *et al.*, 2014; Li *et al.*, 2016; Peng *et al.*, 2017; Liu *et al.*, 2018). In recent years, many studies have focused on defining the chemical compositions and sources of PM$_{2.5}$ (Bahadur *et al.*, 2009; Chen *et al.*, 2010; Yang *et al.*, 2011; Tao *et al.*, 2014; Fang *et al.*, 2017; Dai *et al.*, 2018; Deng *et al.*, 2018).

Receptor models have been very useful tools for PM source apportionments (Khan *et al.*, 2015). For example, Fang *et al.* (2017) identified sources of ambient PM in Haikou, China, using the CMB model; Deng *et al.* (2018) conducted source apportionment of PM$_{2.5}$ in Lin'an, China, using the PCA/MLR model; Liu *et al.* (2017b) apportioned the emission sources of air pollutants using the PMF and ME2 models in Tian'jin, China; and Wang *et al.* (2015) identified the sources of fine particles in Xi'an, China, using the PMF model. The PMF model does not need input source profiles data in the calculation process, which has been widely used to identify PM sources due to the lack of source profiles and the complexity of the sources (Okuda *et al.*, 2010; Xu *et al.*, 2012; Zhu *et al.*, 2012; Chen *et al.*, 2014). However, the choice of factor number in the PMF calculation process can have a critical impact on the apportionment results. In the PMF 5.0 model, the optimal factor solutions can be identified by three error estimation methods (Liu *et al.*, 2017a). The uncertainty of PMF analysis derived from the rotational ambiguity and random errors can be obtained

---

* Corresponding author.

E-mail address: bixh@nankai.edu.cn

by error estimation (EE) methods; the uncertainty of each factor's identifying species is shown to be a useful gauge for evaluating multiple solutions, e.g., with a different number of factors (Brown *et al.*, 2015). Therefore, the EE methods can play an important guiding role in choosing an optimal factor solution. For example, Paatero *et al.* (2014) and Liu *et al.* (2017a) had applied the EE method to choose an optimal factor solution and obtained the good results. However, the related research on source apportionments using the PMF model with EE methods is still limited.

Tian'jin, a rapidly developing megacity in China, had a permanent population of over 15 million and over 2.83 million automobiles in 2016 (Tian'jin Statistical Yearbook 2017; http://stats.tj.gov.cn/Category_29/Index.aspx). The heating period in Tian'jin normally begins on 15 November, after which coal combustion for heating can increase the level of air pollution (Yu *et al.*, 2010; Huang *et al.*, 2014), and heavy pollution events become more frequent along with unfavorable meteorological conditions (Yang *et al.*, 2016; Liu *et al.*, 2018). According to 2016 monitoring data, the mean concentrations of PM_{10} and $PM_{2.5}$ during the heating period in Tian'jin reached 97 and 66 $\mu g\ m^{-3}$, 0.9 and 1.6 times higher than the World Health Organization (WHO) 24-h guideline value of 50 and 25 $\mu g\ m^{-3}$. Given this serious pollution, understanding the chemical compositions and sources of the PM is very important for implementing effective control measures. Although source apportionments of atmospheric particulates in Tian'jin have been conducted in the past (Gu *et al.*, 2011; Zhang *et al.*, 2011; Wu *et al.*, 2015), the recent implementation of pollution control measures may lead to changes in the compositions and sources of PM, and current knowledge is limited. In addition, the distribution for pollution sources in different regions in one city is obviously different; thus, more detailed spatial source apportionment is also needed in order to control these sources more accurately.

Therefore, in this study we aimed to: (1) better understand pollution levels in Tian'jin during the heating period; (2) characterize the concentration variations of PM_{10} and $PM_{2.5}$ and their chemical species; (3) reveal optimal factor solutions using EE analysis and apportion source contributions using the PMF model; and (4) identify the transport pathway of air masses and potential source areas of PM_{10} and $PM_{2.5}$ using backward trajectory and PSCF analysis, respectively.

These results can provide some data support for Tian'jin's municipal government departments to control atmosphere PM sources more accurately.

MATERIALS AND METHODS

Site Description

Tian'jin (38.57–40.25° N, 116.72–118.01° E), one of the megacities in the Bei'jing-Tian'jin-He'bei area, has an area of ~12,000 km^2. The area has a temperate monsoon climate, with an average annual temperature of 11.4–12.9°C and an annual precipitation of 520–660 mm. Southwest, northwest, and northeast winds prevail during summer and autumn, while northwest and northeast winds prevail during spring and winter (Liu *et al.*, 2016b). We collected ambient $PM_{2.5}$ samples at six sites (NJ, NK, DZG, ADR, QJ, and FK;

Fig. 1) set on building rooftops ~9–15 m above ground level; further details are given in Table S1. The data of gaseous pollutants was collected from nearby National or Provincial Air Quality Monitoring Stations (within 10 m). The mean concentrations of SO_2, NO_2, O_3, and CO were 34 $\mu g\ m^{-3}$, 52 $\mu g\ m^{-3}$, 43 $\mu g\ m^{-3}$, and 1.2 $mg\ m^{-3}$ during the study period, respectively, with clear spatial variations (Table S2).

Ambient Sampling and Analysis

From 22 February to 2 March 2016, we used four medium-volume samplers (TH-150C; Wuhan Tianhong Ltd., China) to collect PM_{10} and $PM_{2.5}$ samples at each site for 23 h (from 10:00 a.m. to 9:00 a.m. the next day) at a flow rate of 100 L min^{-1}. Multiple filters were applied to synchronously collect ambient $PM_{2.5}$ samples; parallel samples and field blanks were also collected at each site. Finally, a total of 14 $PM_{2.5}$ and 14 PM_{10} samples (including the parallel and blank samples) were collected at each site, respectively. A total of 84 $PM_{2.5}$ and 84 PM_{10} samples were collected at six sites during the sampling period. In order to better determine the representative of sampling time for the heating period, we analyzed the trends of six air pollutants (i.e., $PM_{2.5}$, PM_{10}, SO_2, NO_2, CO, and O_3) during the heating period in 2016, and the results were described in Fig. S1. The sampling period in this study can basically include the peak and trough periods of air pollutant concentration changes; therefore, the sampling period is representative for the heating period.

Polypropylene membrane filters were used to determine chemical elements (Na, Fe, V, Mg, K, Ca, Mn, Ti, Cr, Cd, Ni, As, Cu, Pb, Zn, Al, and Si) by inductively coupled plasma atomic emission spectrometry (ICP-AES) (IRIS Intrepid II; Thermo Electron). Quartz fiber filters were used to determine SO_4^{2-}, NO_3^-, Cl^-, NH_4^+, Na^+, K^+, Mg^{2+}, and Ca^{2+} by ion chromatography (DX-120; Dionex). A circular quartz fiber filter of 0.210 cm^2 was used to measure elemental carbon (EC) and organic carbon (OC) using a Desert Research Institute Model 2001 thermal/optical carbon analyzer with the IMPROVE A thermal/optical reflectance protocol. The method detection limits of chemical species, water-soluble inorganic ions, and carbonaceous species are listed in Table S3. Further details regarding sampling, measurement, and quality control are given in the supplementary material.

PMF and Error Estimation Model

PMF is a multivariate factor analysis tool widely used for PM source apportionment (Liu *et al.*, 2017a, 2018). This model can decompose a matrix of speciated sample data (X) into two matrices: factor contributions (G) and factor profiles (F) (Paatero and Tapper, 1994). The speciated data are the matrix X of *i* by *j* dimensions, in which *i* number of samples and *j* chemical species were measured; further context is given in the supplementary material. We used three EE methods to choose optimal factor solutions: displacement of factor elements (DISP), classical bootstrap (BS), and bootstrap enhanced by displacement (BS-DISP). Further details were given in Liu *et al.* (2017a).

Backward Trajectory and PSCF Models

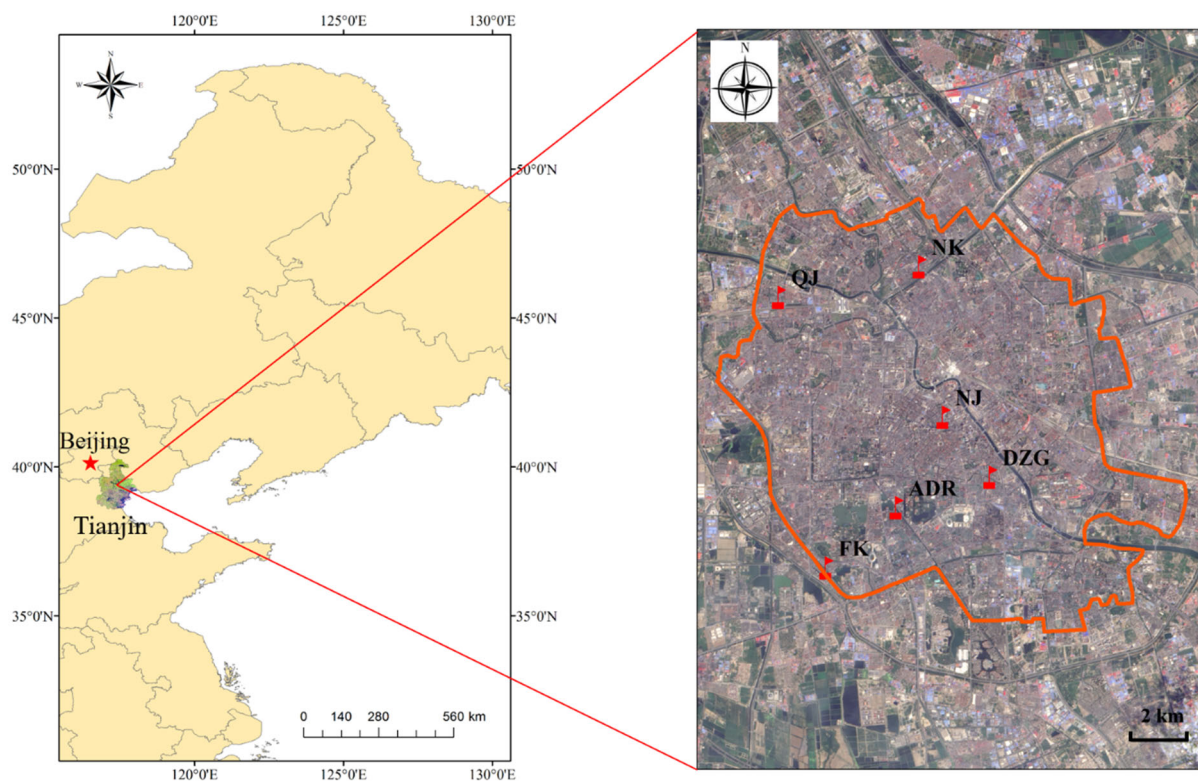The 72-h backward trajectories from the center of Tian'jin

Fig. 1. Locations of the sampling sites in Tian'jin. NJ: Nanjing Road, NK: Nankou Road, DZG: Dazhigu Road, ADR: Advancing Road, QJ: Qinjian Road, FK: Fukang Road.

(39.13°N, 117.20°E) were calculated at 1-h intervals during the sampling period. The final global analysis data were produced by the National Centers for the Global Data Assimilation System (GDAS; http://www.arl.noaa.gov/). The backward trajectory model was performed four times per day at starting times of 0:00, 06:00, 12:00, and 18:00 LT at a starting height of 100 m above the ground (Byčenkienė *et al.*, 2014; Liu *et al.*, 2016a, b). The PSCF model combines backward trajectory calculation and air pollutant concentrations for identifying potential source areas. All hourly endpoints from the backward trajectories were classified into $1° \times 1°$ latitude and longitude grid cells; further details are given in the supplementary material.

RESULTS AND DISCUSSION

PM_{10} and $PM_{2.5}$ Concentrations

During the heating period, the concentrations of PM_{10} and $PM_{2.5}$ ranged between 37–262 μg m^{-3} and between 17–214 μg m^{-3}, respectively (Fig. 2); the mean $PM_{2.5}/PM_{10}$ ratio was 0.67. The average PM_{10} and $PM_{2.5}$ concentrations of 98 and 71 μg m^{-3} exceeded Chinese air quality standards by 140% and 203%, respectively, as well as the stricter World Health Organization air quality guidelines of 20 and 10 μg m^{-3}, respectively (World Health Organization, 2006). The PM_{10} and $PM_{2.5}$ concentrations showed significant spatial differences (*t*-test, $p < 0.05$) with standard deviations of up to 12 and 6 μg m^{-3}, respectively. A higher PM_{10} concentration was observed at NK (108 μg m^{-3}), with a relatively low $PM_{2.5}/PM_{10}$ ratio (0.60), likely indicating that crustal dust had an important

influence here (Shakya *et al.*, 2017). Lower PM_{10} (94 μg m^{-3}) and higher $PM_{2.5}$ (78 μg m^{-3}) concentrations were observed at QJ along with a higher $PM_{2.5}/PM_{10}$ ratio (0.78), likely indicating important contributions of fine-particle emission sources such as vehicles and secondary inorganic aerosol, as QJ was characterized by traffic and residential areas where the influence of vehicle emissions would be relatively high (Table S1). The mass concentrations of PM_{10} and $PM_{2.5}$ at each site showed increasing trends from February to March, likely due to the heavy pollution event in March (Fig. 2). Compared with other regions around the world (Table S4), we found that the mean $PM_{2.5}$ and PM_{10} concentrations in Tian'jin were usually higher than some cities in Europe and Korea, but apparently lower than many cities in Beijing-Tianjin-Hebei and surrounding areas. From 2008 to 2013, the concentration of $PM_{2.5}$ in Tian'jin showed an increasing trend (Gu *et al.*, 2011; Wu *et al.*, 2015). Subsequently, the $PM_{2.5}$ concentration decreased significantly (Tian *et al.*, 2018; Yan *et al.*, 2018), which might be closely associated with the Air Pollution Prevention and Control Action Plan issued by China in 2013 (http://www.gov.cn/jrzg/2013-09/12/content _2486918.htm). The control measures of PM sources were tightened in Tian'jin so that the PM concentrations can decrease significantly.

Characteristics of Chemical Species in PM
Water-soluble Ions

The average concentrations of the SNA (the sum of SO_4^{2-}, NO_3^-, and NH_4^+) in PM_{10} and $PM_{2.5}$ reached 23.4 and 19.9 μg m^{-3}, respectively, accounting for 72.4% and 77.1%
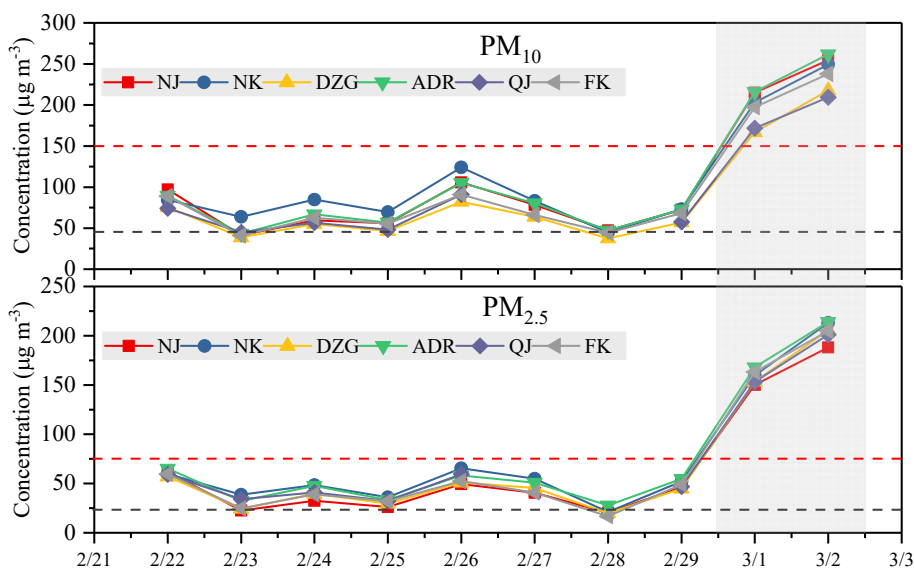
Fig. 2. Temporal variations of PM_{10} and $PM_{2.5}$ concentrations at six sampling sites during the heating period. The grey shadows represent the pollution episode.

of the total measured ions, and 23.9% and 28.0% of PM_{10} and $PM_{2.5}$. The mean concentrations of NO_3^-, SO_4^{2-}, Cl^-, and NH_4^+ in PM_{10} were 12.4, 7.1, 3.8, and 3.9 µg m^{-3}, accounting for 12.6%, 7.2%, 3.9%, and 4.0% of PM_{10} concentrations, respectively. The mean concentrations of NO_3^-, SO_4^{2-}, Cl^-, and NH_4^+ in $PM_{2.5}$ were 10.5, 5.7, 3.1, and 3.7 µg m^{-3}, accounting for 14.8%, 8.0%, 4.3%, and 5.2% of $PM_{2.5}$ concentrations, respectively. The concentrations and percentages of NO_3^- in $PM_{2.5}$ and PM_{10} were significantly higher than other measured ions (t-test, $p < 0.01$). The nitrate is mainly produced from secondary reactions of nitrogen oxide emitted from motor vehicles, coal combustion, and industrial emissions (Liu *et al.*, 2016a; He *et al.*, 2017), likely implying that these sources had larger contributions to $PM_{2.5}$ and PM_{10} during the heating period. The ratio of SO_4^{2-} in $PM_{2.5}$ to that in PM_{10} (0.80), along with those of NO_3^- (0.85), NH_4^+ (0.94), and Cl^- (0.80), suggested that these measured ions were mainly enriched in fine particles.

The concentrations of the predominant water-soluble ions in PM_{10} and $PM_{2.5}$ at all sampling sites showed the same tendency and decreased in the order: NO_3^- (8.2–17.4 µg m^{-3}) > SO_4^{2-} (4.7–9.5 µg m^{-3}) > NH_4^+ and Cl^- (2.0–5.0 µg m^{-3}) (Fig. S2). The concentrations of NO_3^- (15.7–17.4 µg m^{-3}), SO_4^{2-} (8.0–9.5 µg m^{-3}), and Cl^- (3.9–5.0 µg m^{-3}) were highest at QJ, consistent with higher $PM_{2.5}$ concentrations at that site. SO_4^{2-} and NO_3^- are mainly formed by secondary reactions of sulfur dioxide and nitrogen oxide emitted from coal combustion and vehicles (Almeida *et al.*, 2015; Liu *et al.*, 2016a). Wet-process desulfurization from coal-fired power plants can also directly discharge abundant sulfate particles into the air (Ma *et al.*, 2015; Liu *et al.*, 2017a). Cl^- is another indicator of coal combustion (Wu *et al.*, 2015), suggesting that QJ was primarily affected by coal combustion and vehicle emissions. By contrast, the concentrations of SO_4^{2-} (4.7–5.6 µg m^{-3}), Cl^- (2.8–3.7 µg m^{-3}), and NO_3^- (8.2–9.0 µg m^{-3}) were lowest at ADR, implying lower contributions of coal combustion and vehicle emissions, perhaps because that site

was characterized by residential, commercial, and scenic areas (Table S1).

The sulfur and nitrogen oxidized ratios (SOR and NOR, respectively) were calculated by the molar ratios of $[SO_4^{2-}]$ to $[SO_4^{2-} + SO_2]$ and $[NO_3^-]$ to $[NO_3^- + NO_2]$, respectively (Dai *et al.*, 2018). The average values of SOR and NOR in PM_{10} during the heating period were 0.17 and 0.14, respectively, while those for $PM_{2.5}$ were 0.13 and 0.12, respectively. All were higher than 0.1, indicating the formation of secondary species (Truex *et al.*, 1980; Zhang *et al.*, 2013). Higher average values of SOR (0.20–0.22) and NOR (0.16) and a higher O_3 concentration (39 µg m^{-3}) were observed at QJ (Table S2), likely implying stronger oxidation of SO_2 to SO_4^{2-} and NO_2 to NO_3^-, which could have an important influence on the high concentrations of SO_4^{2-} and NO_3^- at this site (Fig. S2). The mean values of SOR (0.05–0.12) and NOR (0.04–0.08) were lower at ADR, likely due to the lower O_3 concentration (25 µg m^{-3}) (Table S2). Gao *et al.* (2011), Zhou *et al.* (2016), and Zhang *et al.* (2013) found that average winter SOR values in Ji'nan, Shang'hai, and Fu'zhou were 0.17, 0.20, and 0.22–0.27, while those for NOR were 0.12, 0.12, and 0.05–0.08, respectively—all higher than those in Tian'jin.

The average SO_4^{2-}/NO_3^- ratios were 0.57 and 0.54 for PM_{10} and $PM_{2.5}$ during the heating period, respectively. The mass ratio of SO_4^{2-}/NO_3^- can reflect the relative importance of stationary versus mobile sources of sulfur and nitrogen in the atmosphere (Liu *et al.*, 2017a; Murillo *et al.*, 2012). The mean ratio of SO_4^{2-}/NO_3^- (1.0) was highest at NK, and the SO_4^{2-} concentration was higher (Fig. S2), suggesting that the influence of stationary sources might be larger here (Table S1). The average ratio of SO_4^{2-}/NO_3^- (0.5–0.6) at QJ was lower, and the NO_3^- concentration was higher, indicating that the contribution of mobile sources was larger at this site (Table S1). The SO_4^{2-}/NO_3^- ratios showed a decreasing tendency with increasing PM_{10} and $PM_{2.5}$ concentrations (*slope* = –0.004 and r = –0.70 for PM_{10}; *slope* = –0.005 and r = –0.77 for

$PM_{2.5}$) (Fig. S3), likely implying that mobile sources could have had an important impact on the increase of PM_{10} and $PM_{2.5}$ concentrations (Liu *et al.*, 2017a).

The correlations between NH_4^+ and both NO_3^- and SO_4^{2-}; ($r = 0.64–0.81$, $p < 0.01$) were higher than that between NH_4^+ and Cl^- ($r = 0.37–0.43$, $p < 0.01$) (Table S5), indicating that NH_4^+ might exist in the form of ammonium sulfate, ammonium hydrogen sulfate, and ammonium nitrate during the heating period (Wang *et al.*, 2005). There were significant correlations between NO_3^- and SO_4^{2-} ($r = 0.73–0.82$, $p < 0.01$), reflecting higher homology. The correlation between Ca^{2+} and Mg^{2+} was higher in PM_{10} ($r = 0.71$, $p < 0.01$) than $PM_{2.5}$ ($r = 0.54$, $p < 0.05$), suggesting that they might be derived mainly from sources of coarse particles such as dust. In addition, the correlation between K^+ and Cl^- was higher in $PM_{2.5}$ ($r = 0.81$, $p < 0.01$) than PM_{10} ($r = 0.56$, $p < 0.01$), probably indicating that they mainly originated from sources of fine particles such as biomass burning. Meanwhile, potassium chloride might be an important form of Cl^- during the heating period.

Carbonaceous Materials

The average concentrations of OC and EC in PM_{10} were 11.8 and 3.9 µg m^{-3} during the heating period, respectively—significantly higher than those in $PM_{2.5}$ (9.4 and 3.0 µg m^{-3}; *t*-test, $p < 0.01$). The percentages of OC and EC in PM_{10} were 12.0% and 4.0%, respectively, lower than those in $PM_{2.5}$ (13.2% and 4.2%), indicating these carbonaceous materials were mainly enriched in $PM_{2.5}$. Note that the concentrations and percentages of SNA in PM were apparently higher than those of total carbon (TC; the sum of OC and EC). The concentrations and percentages of OC in PM were close to those of NO_3^- but significantly higher than other water-soluble ions (*t*-test, $p < 0.01$). The NO_3^- and OC have become the dominant components of particulate matter at present. The higher correlations between OC and EC ($R^2 = 0.87–0.93$) (Fig. S4) suggest that they might be derived from the same sources (Liu *et al.*, 2016c). The correlations between OC and EC did not differ statistically between the sampling sites, except for NK (Fig. 3), likely implying similar sources of carbonaceous materials. The correlations between OC and
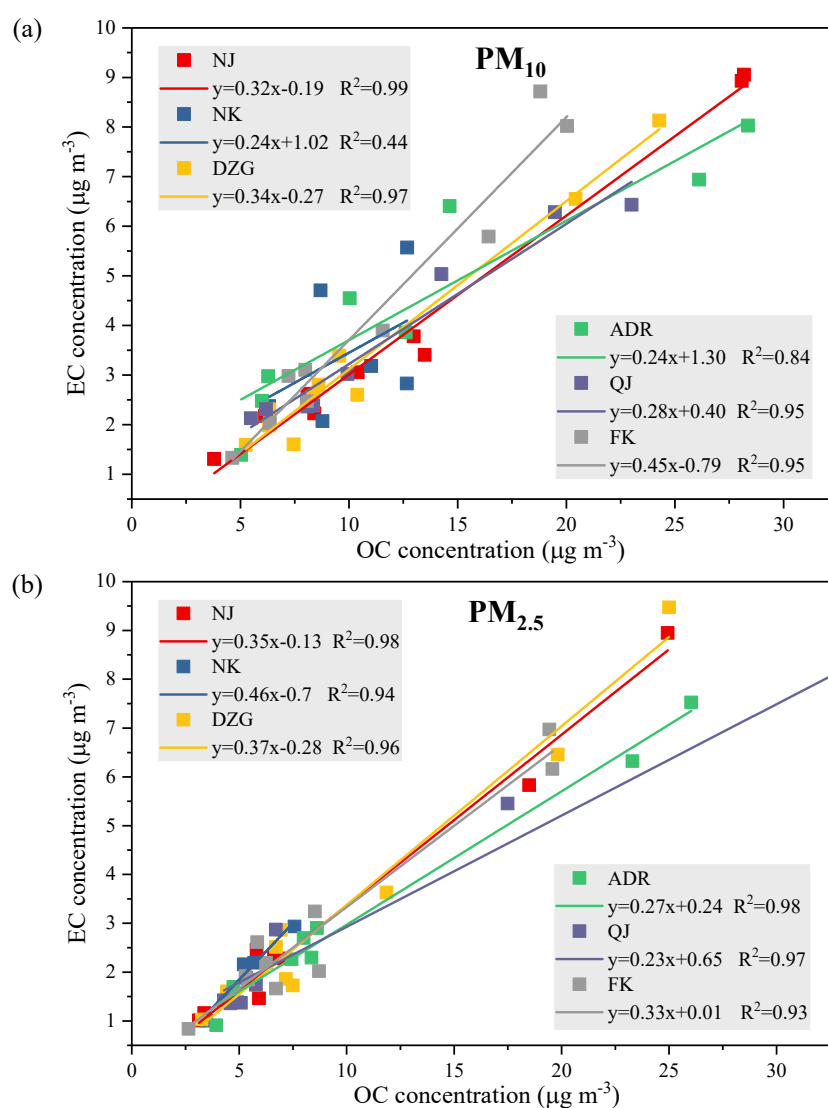

Fig. 3. Correlations between OC and EC in (a) PM_{10} and (b) $PM_{2.5}$ at different sampling sites.

EC were higher at NJ (r = 0.98–0.99) and lower at NK (r = 0.44–0.94), indicating the high homology of OC and EC at the former. The sources of OC and EC at NK might be complex because this site was located in industrial and traffic areas (Table S1). The OC/EC average ratios in PM_{10} and $PM_{2.5}$ during the heating period were 3.1 and 3.2, respectively. The mean OC/EC ratios by site showed little spatial differences (Table S6), ranging from 2.8 (FK) to 3.3 (NJ and DZG) for PM_{10} and 2.8 (NK) to 3.4 (ADR) for $PM_{2.5}$. Other studies have reported that the OC/EC ratios from biomass burning, coal combustion, and vehicle exhaust were 4.1–14.5, 0.3–7.6, and 1.0–4.2, respectively (Watson *et al.*, 2001; Schauer *et al.*, 2002; Liu *et al.*, 2016a; Zhang *et al.*, 2007). Therefore, the contributions of coal combustion and vehicle emission might be relatively high during the heating period.

An OC/EC ratio larger than 2.0–2.2 has been used to identify and evaluate secondary organic aerosols (SOAs) (Turpin and Huntzicker, 1991; Chow *et al.*, 1996). In Tian'jin, the average OC/EC ratio during the heating period was 3.1 and 3.2 for PM_{10} and $PM_{2.5}$, respectively, indicating the possible presence of SOAs. The SOC is calculated using the EC-tracer method (Gu *et al.*, 2010):

$$SOC = OC - EC \times (OC/EC)_{min} \qquad (1)$$

Linear regression parameters of OC and EC based on different percentiles of OC/EC ratios are shown in Tables S7–S13. The regression of OC and EC data below 10th percentile of OC/EC ratios shows the best solution to calculate the $(OC/EC)_{min}$ ratio. In this study, the observed $(OC/EC)_{min}$ values during the heating period were 1.8 and 2.2 in PM_{10} and $PM_{2.5}$, respectively, and the average SOC concentrations were 4.8 and 2.8 $\mu g\ m^{-3}$, respectively (Table S6). The fractions of SOC to OC mass were 39.8% and 28.0% in PM_{10} and $PM_{2.5}$, respectively (Table S6), which could indicate an important contribution to particle matter. Relatively high SOC concentrations in PM_{10} were observed at ADR (4.0 $\mu g\ m^{-3}$) and NK (3.8 $\mu g\ m^{-3}$), while the SOC concentration at DZG (1.6 $\mu g\ m^{-3}$) was relatively low. A higher SOC concentration in $PM_{2.5}$ was observed at NK (3.8 $\mu g\ m^{-3}$), and a lower SOC concentration was found at QJ (0.5 $\mu g\ m^{-3}$).

Elements

Seventeen elements (Na, Fe, V, Mg, K, Ca, Mn, Ti, Cr, Cd, Ni, As, Cu, Pb, Zn, Al, and Si) in PM_{10} and $PM_{2.5}$ were determined during the heating period; the concentrations of the total detected elements in PM_{10} and $PM_{2.5}$ were 12.4 and 6.4 $\mu g\ m^{-3}$, respectively, accounting for 12.7% and 9.0% of the PM_{10} and $PM_{2.5}$ mass, respectively. Crustal elements (Mg, Al, K, Si, Na, Ca, and Fe) were the most abundant elements, accounting for 73.2–84.2% of the total detected elemental mass, similar to the results of Mohammed *et al.* (2017) and Liu *et al.* (2017a). The average concentrations of Mg, Al, K, Si, Na, Ca, and Fe in PM_{10} were 0.9, 1.3, 1.0, 3.2, 0.3, 3.4, and 1.9 $\mu g\ m^{-3}$, respectively—significantly higher than those in $PM_{2.5}$. The mass ratios of Mg, Al, Si, Ca, and Fe in $PM_{2.5}$ to those in PM_{10} were 0.44, 0.48, 0.47, 0.45, and 0.44, respectively, indicating that these elements were mainly enriched in PM_{10}. The total concentrations of crustal elements

at different sites showed apparent differences (*t*-test, $p <$ 0.05). The higher concentrations were observed at NK (7.3–13.4 $\mu g\ m^{-3}$), likely suggesting that the influence of crustal sources around that site was higher than at other sites. The lower concentrations were found at FK (3.5–10.6 $\mu g\ m^{-3}$), probably because this site was situated in the city center and crustal sources were relatively scarce (Fig. 1). The trace elements (V, Mn, Ti, Cd, Ni, As, Cu, Pb, and Zn) accounted for a small part of the total detected elements.

The enrichment factors (EFs) relative to the composition of Earth's upper crust were used to identify anthropogenic influences on the PM-related elements (Rogula-Kozłowska *et al.*, 2012; Zhang *et al.*, 2015), using Al as a reference element (Liu *et al.*, 2016a). The concentrations of elements in the crust refer to their content in the topsoil in China (SEPA, 1990). The EFs were calculated as follows:

$$EF_x = \frac{(C_X/C_R)_{aerosol}}{(C_X/C_R)_{crust}} \qquad (2)$$

where $(C_X/C_R)_{aerosol}$ is the ratio of X to R in the aerosol and $(C_X/C_R)_{crust}$ is the ratio of X to R in the crust. The average EFs of elements in PM_{10} and $PM_{2.5}$ at different sampling sites are shown in Fig. 4 and Figs. S5–S6. The EF level of selected trace metals varied similarly at each site. The EF values for As, Ca, Cd, Cu, Ni, Pb, and Zn were > 10, indicating that they were closely associated with human activities such as vehicle emissions and metal manufacturing (Zhang *et al.*, 2010, 2015). The mean EF values for Na and Ti were close to 1 at each site, suggesting that they originated mainly from crustal sources (Xu *et al.*, 2013). The EF values for Ca varied from 14–21 at different sites, which might be affected by diverse sources such as construction activity and crustal sources (Almeida *et al.*, 2015; Liu *et al.*, 2016a). The EF value of K in $PM_{2.5}$ was less than 5 at each site, likely due to the influence of crustal sources, while the impact of anthropogenic sources such as biomass burning might be relatively low.

Source Apportionment
EE Analysis

EE diagnostics are summarized in Tables S14–S15. In moving from two to eight factors, the Q/Q_{except} of PM_{10} and $PM_{2.5}$ decreased from 8.1 to 3.3 and 9.0 to 3.4, respectively, along with a smaller decrease when moving from five to six factors (4.5 to 4.2 for PM_{10} and 5.1 to 4.5 for $PM_{2.5}$). When changes in Q values become small with increasing factors, it can suggest that there may be too many factors being fit, indicating that five factors can be an optimal solution (Brown *et al.*, 2015). Our results were generally stable at five factors, with all factors mapped in BS in 100% of runs and no swaps occurring with DISP. Thus, five factors (F_{peak} = 0, seed = 16 for PM_{10}, seed = 2 for $PM_{2.5}$) were selected for PMF analysis. The range of all scaled residuals was between –2 and 2. The calculated PM mass concentrations from the PMF model and observed PM mass concentrations showed higher correlations (*slope* = 0.95 and R^2 = 0.94 for PM_{10}; *slope* = 0.96 and R^2 = 0.95 for $PM_{2.5}$) (Fig. S7).
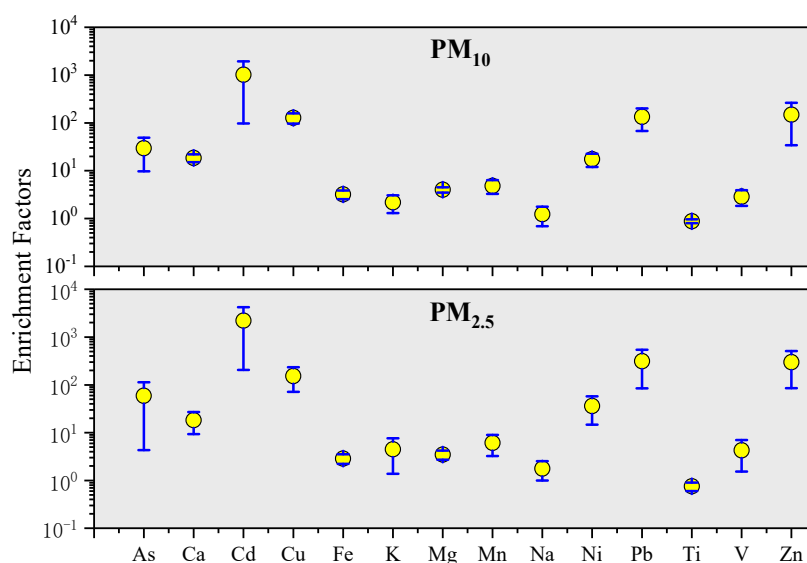
Fig. 4. Enrichment factors of trace elements in PM_{10} and $PM_{2.5}$ during the heating period.

Source Apportionment

Five factors were chosen using the EE analysis and field investigation results during the heating period (Figs. 5–6), and then the PMF model was run based on the chemical species concentration data in PM_{10} and $PM_{2.5}$. The main species defining Factor 1 were SO_4^{2-} (49.8–52.1% of the total SO_4^{2-}), NO_3^- (59.6–77.6%), and NH_4^+ (71.3–83.2%), so this factor was identified as secondary inorganic aerosol (Wang *et al.*, 2006; Contini *et al.*, 2010; Tao *et al.*, 2013; Liu *et al.*, 2016a). Factor 2 was represented by high loadings of OC (24.1–28.5%), EC (3.8–5.3%), K (58.2–74.7%), and Cl^- (17.7–27.8%), which are generally indicators of biomass burning (Heo *et al.*, 2009; Hleis *et al.*, 2013; Lan *et al.*, 2016), so this factor was identified as biomass burning. The chemical profile of Factor 3 was mainly defined by Si (61.6–70.8%), Ca (39.9–66.7%), Mg (47.6–76.8%), Al (52.5–64.1%), and Fe (33.3–65.5%), which are generally derived from crustal dust (Tullio *et al.*, 2008; Almeida *et al.*, 2015; Liu *et al.*, 2016a), so this factor was identified as crustal dust. Factor 4 was represented by high loadings of As (44.2–49.6%), Cl^- (43.3–43.5%), OC (18.1–19.3%), NO_3^- (16.3–27.3%), SO_4^{2-} (16.9–24.8%), Si (21.3–27.7%), Ca (31.6–32.1%), Al (13.7–23.3%), and Mg (23.0–36.9%), which are closely related to coal combustion (Bhangare *et al.*, 2011; Cao *et al.*, 2011; Schleicher *et al.*, 2011; Liu *et al.*, 2016a), so this factor was identified as coal combustion. Factor 5 had relatively high loadings of OC (36.2–43.5%), EC (65.9–66.7%), Cu (35.4–40.4%), and Zn (33.0–51.6%); OC and EC are major pollutants from gasoline and diesel combustion (Liu *et al.*, 2016a), while Zn is usually used as an additive in lubricating oil in two-stroke engines and Cu is linked to brake wear (Begum *et al.*, 2004; Canha *et al.*, 2012; Shafer *et al.*, 2012; Lin *et al.*, 2015). Thus, this factor was identified as vehicle exhaust.

The source apportionment results for PM_{10} and $PM_{2.5}$ are shown in Fig. 7 and Figs. S8–S9. The contributions of secondary inorganic aerosol, coal combustion, crustal dust, vehicle exhaust, and biomass burning to the ambient PM_{10} and $PM_{2.5}$ were 28–30%, 20–21%, 18–21%, 17–20%, and 4%, respectively. Compared to $PM_{2.5}$, the contribution of crustal dust to the ambient PM_{10} was relatively high, while the contribution of vehicle exhaust to PM_{10} was relatively low (Fig. 7). The contributions of secondary inorganic aerosol to the ambient PM_{10} and $PM_{2.5}$ showed little difference. The secondary sulfate was mainly derived from the secondary reaction of SO_2 emitted from coal combustion (Russell *et al.*, 1983; Liu *et al.*, 2013), suggesting that the contributions of coal combustion to the ambient PM_{10} and $PM_{2.5}$ were higher than other sources during the heating period, likely due to space heating in winter. The higher contributions of vehicle exhaust were probably associated with the growing number of automobiles in Tian'jin. Some sources (contributions of 8–10%) were not resolved by the PMF, likely because emission sources are complicated and diverse and there is a lack of actual source profiles, especially for open sources such as garbage combustion and other unorganized sources (Liu *et al.*, 2016a).

Figs. S8–S9 show the results of source apportionment for ambient $PM_{2.5}$ and PM_{10} at different sampling sites during the heating period. The contributions of coal combustion and vehicle exhaust at ADR were lowest, probably because this site was located in scenic and commercial area (Table S1). The contributions of coal combustion and crustal dust at NK were the highest (22–23% and 21–25%, respectively). This site was situated in an industrial area with ongoing construction activity (Table S1). The contributions of vehicle exhaust at QJ and FK were higher than at other sites, likely because these were located in traffic, residential, and scenic areas (Table S1) with higher traffic volume. The contributions of crustal dust at QJ and FK were significantly lower than at other sites. The contributions of secondary inorganic aerosol showed minor differences between sites, with higher contributions at QJ and lower ones at DZG. The contributions of biomass burning were apparently lower than other sources at most sites; the contribution at DZG was significantly higher than at other sites, whose contributions did not differ much.
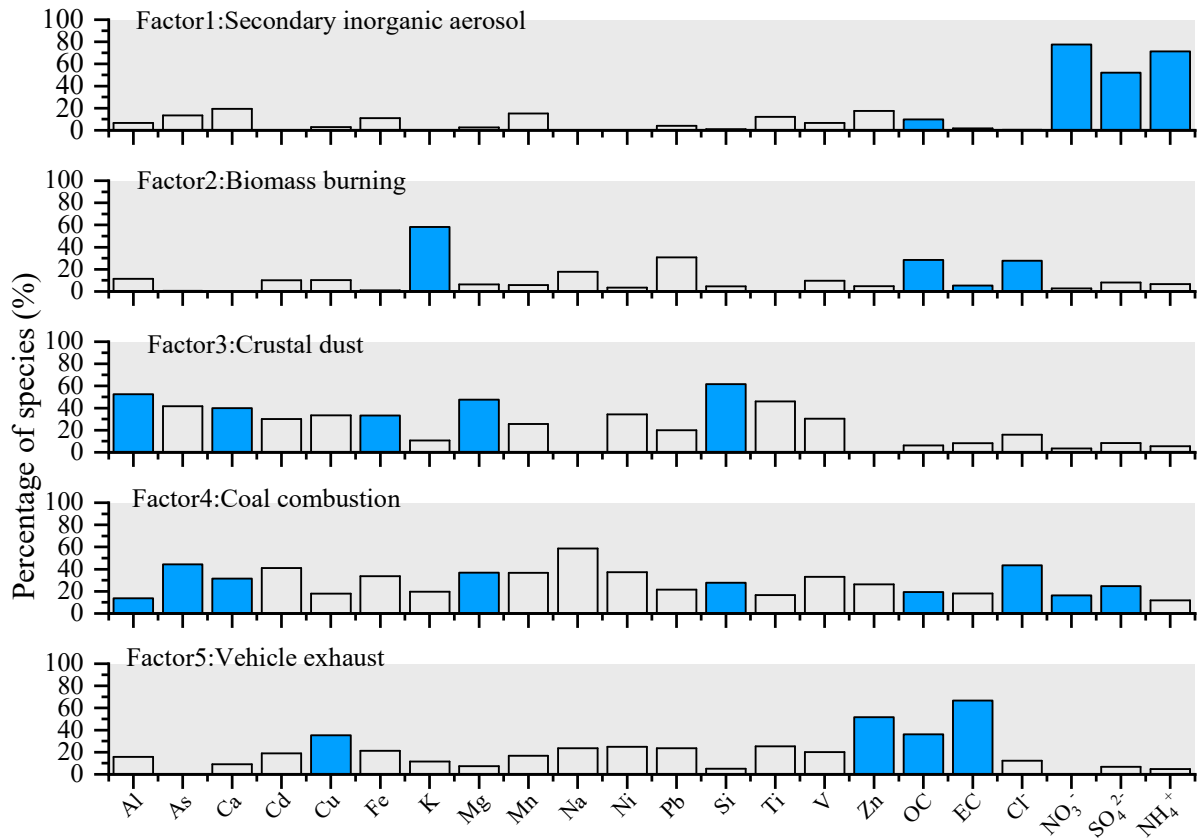
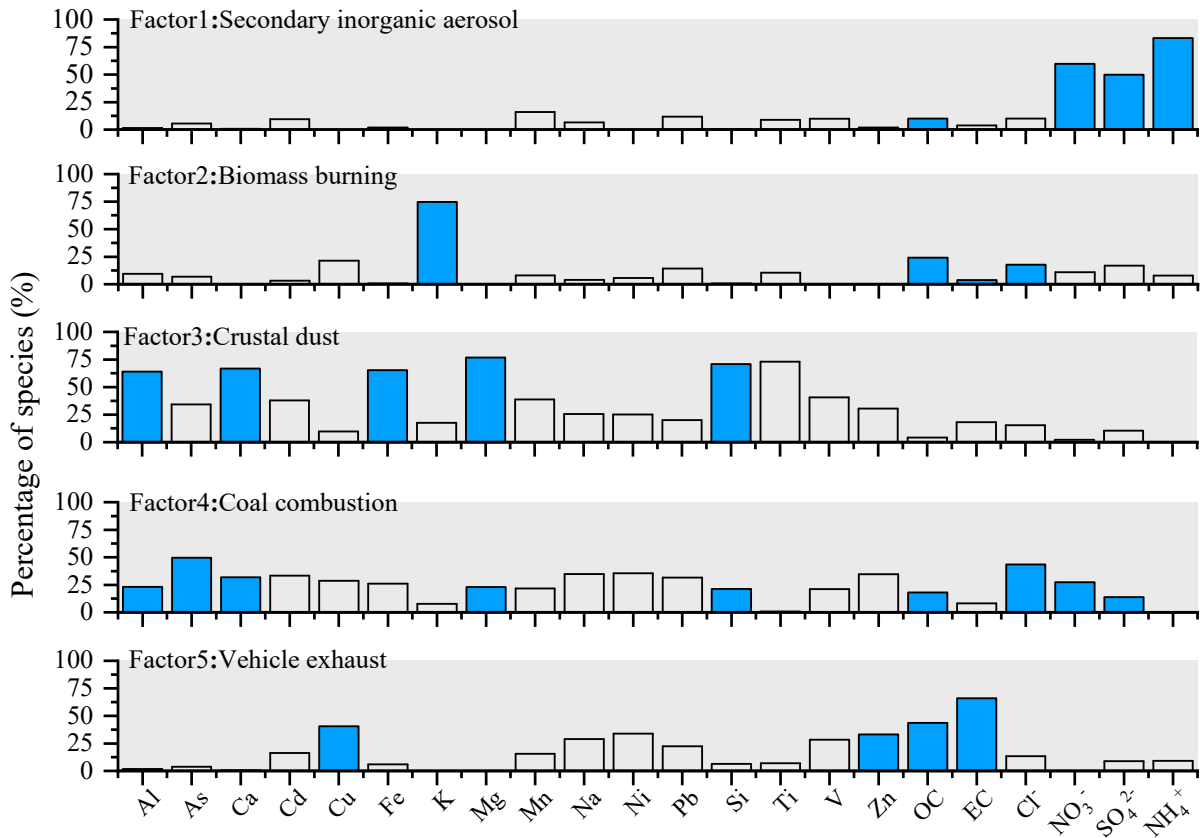**Fig. 5.** Factor profile (% of species) of each source for PM$_{10}$.

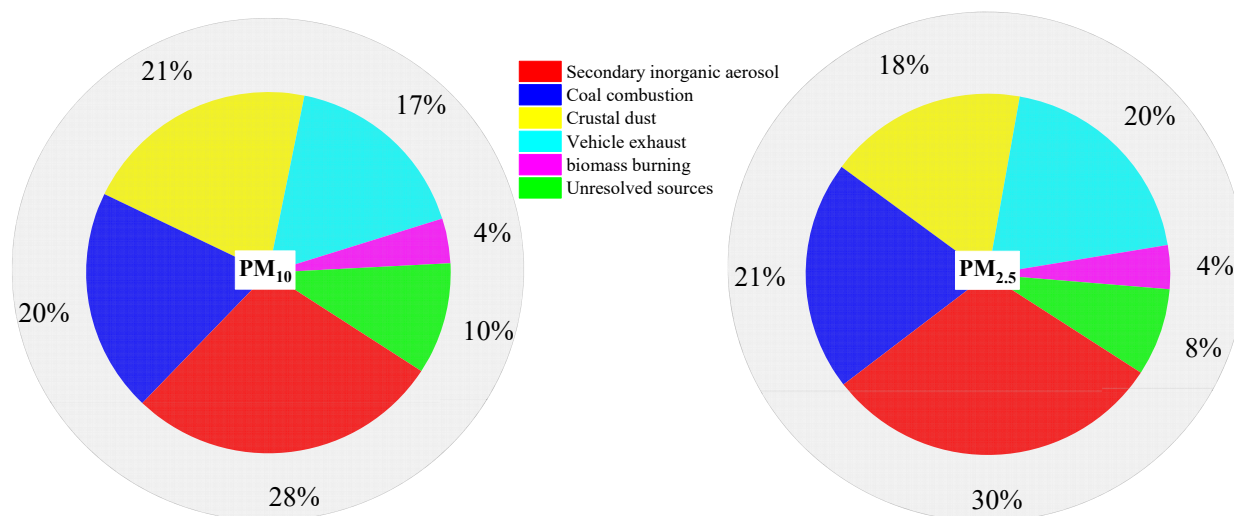**Fig. 6.** Factor profile (% of species) of each source for PM$_{2.5}$.

Fig. 7. The contribution of each source to PM$_{10}$ and PM$_{2.5}$ at the urban area during the heating period.

Similar studies have recently been conducted in many other Chinese cities. For example, Qiu *et al.* (2016) found that dust (26.9–29.8%), secondary aerosols (26.9–28.3%), coal burning (15.7–17.3%), traffic (15.1–16.7%), and industry (8.2–9.0%) were major contributors to the ambient PM$_{10}$ and PM$_{2.5}$ in Lan'zhou. Fang *et al.* (2017) found that resuspended dust (17.5–35.0%), vehicle exhaust (14.9–23.6%), and secondary particulates (20.4–28.8%) were major sources for PM$_{2.5}$ and PM$_{10}$ in Hai'kou. Gu *et al.* (2014) reported that coal combustion and biomass burning (38.0–46.2%), secondary sulfate (35.0–36.9%), and crustal dust (10.2–16.9%) were major sources for PM$_{2.5}$ in Ji'nan. Zhang *et al.* (2017) summarized and analyzed receptor-based source apportionment research on fine-particulate matter in China, finding that secondary inorganic aerosol and traffic emissions had higher contributions in South China while the percentages contributed by coal combustion, dust, and biomass burning to the total PM$_{2.5}$ were higher in North China. Although our results were broadly consistent with Zhang *et al.* (2017), major sources and contributions of ambient particulate matter still differ between cities, likely due to different economic development patterns, individual industrial and energy structures, and patterns of human activity (Liu *et al.*, 2016a, 2017a).

Backward Trajectory and PSCF Analysis

We used backward trajectory analysis to reveal the transport pathways of the air masses affecting Tian'jin (Fig. 8) and used the PSCF model to identify potential source areas of PM$_{2.5}$ and PM$_{10}$ (Fig. S10). In terms of direction and travelled region, all trajectories were divided into three groups during the heating period. Trajectory Clusters (1), (2), and (3) accounted for 40.0%, 47.5%, and 12.5% of the total trajectories, respectively. Clusters (1) and (2) represented long-range transport patterns, being mainly derived from Mongolia before crossing Inner Mongolia, He'bei, and Bei'jing to reach Tian'jin. Cluster (3) represented a shorter-range transport pattern, mainly originating in Inner Mongolia before passing through Shan'xi and He'bei Provinces to reach Tian'jin. Overall, Tian'jin was mainly influenced by the transport of
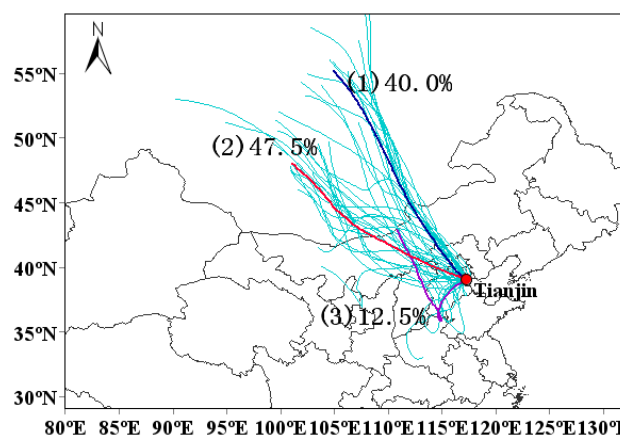

Fig. 8. Analytical results of the 72-h air mass back trajectories at 100 m elevation during the heating period. Three trajectories were calculated based on the trajectory clustering results at Tian'jin.

air masses originating to the northwest during the heating period. Northeastern He'nan, southwestern Shan'dong, Bei'jing, and Tian'jin itself were identified as the potential source areas of PM$_{10}$ and PM$_{2.5}$ using the PSCF model (Fig. S10).

CONCLUSIONS

The mean PM$_{10}$ and PM$_{2.5}$ concentrations in Tian'jin, China, during the 2016 heating season were 98 and 71 µg m^{-3}, and the mean PM$_{2.5}$/PM$_{10}$ ratio was 0.67. The concentrations for both fractions exhibited significant spatial differences, with standard deviations of 6–12 µg m^{-3}. NO$_3^-$ and OC were dominant in the ambient PM$_{2.5}$ and PM$_{10}$, with concentrations and mass percentages significantly exceeding those of the other components. The average SNA concentrations were 19.9–23.4 µg m^{-3}, accounting for 72.4–77.1% of the total measured ions. The SO$_4^{2-}$/NO$_3^-$ ratio showed a decreasing tendency as the particle concentrations increased, implying

a strong influence from mobile sources. The mean OC/EC ratios for PM$_{10}$ and PM$_{2.5}$ were 3.1 and 3.2, respectively, with small spatial differences. The most abundant elements were crustal and were mainly enriched in the PM$_{10}$.

Based on EE diagnostics, five factors for the PM$_{2.5}$ and PM$_{10}$ were selected via PMF analysis: secondary inorganic aerosol, coal combustion, crustal dust, vehicle exhaust, and biomass burning, which contributed 28–30%, 20–21%, 18–21%, 17–20%, and 4%, respectively. Secondary inorganic aerosol displayed less spatial heterogeneity than the other sources in its contributions. Backward trajectory and PSCF analysis showed that air masses affecting Tian'jin mainly originated in the northwest during the heating period, and northeastern He'nan, southwestern Shan'dong, Bei'jing, and Tian'jin itself were major potential source areas.

ACKNOWLEDGMENTS

SUPPLEMENTARY MATERIAL

Supplementary data associated with this article can be found in the online version at http://www.aaqr.org.

REFERENCE

Almeida, S.M., Lage, J., Fernández, B., Garcia, S., Reis, M.A. and Chaves, P.C. (2015). Chemical characterization of atmospheric particles and source apportionment in the vicinity of a steelmaking industry. *Sci. Total Environ.* 521–522: 411–420.

Bahadur, R., Habib, G. and Russell, L.M. (2009). Climatology of PM$_{2.5}$ organic carbon concentrations from a review of ground-based atmospheric measurements by evolved gas analysis. *Atmos. Environ.* 43: 1591–1602.

Begum, B.A., Kim, E., Biswas, S.K. and Hopke, P.K. (2004). Investigation of sources of atmospheric aerosol at urban and semi-urban areas in Bangladesh. *Atmos. Environ.* 38: 3025–3038.

Bhangare, R.C., Ajmal, P.Y., Sahu, S.K., Pandit, G.G. and Puranik, V.D. (2011). Distribution of trace elements in coal and combustion residues from five thermal power plants in India. *Int. J. Coal Geol.* 86: 349–356.

Brown, S.G., Eberly, S., Paatero, P. and Norris, G.A. (2015). Methods for estimating uncertainty in PMF solutions: Examples with ambient air and water quality data and guidance on reporting PMF results. *Sci. Total Environ.* 518–519: 626–635.

Byčenkienė, S., Dudoitis, V. and Ulevicius, V. (2014). The use of trajectory cluster analysis to evaluate the long-range transport of Black Carbon Aerosol in the South-Eastern Baltic region. *Adv. Meteorol.* 2014: 137694.

Canha, N., Freitas, M.C., Almeida-Silva, M., Almeida, S.M., Dung, H.M., Dionísio, I., Cardoso, J., Pio, C.A., Caseiro, A., Verburg, T.G. and Wolterbeek, H.T. (2012). Burn wood influence on outdoor air quality in a small village: Foros de Arrão, Portugal. *J. Radioanal. Nucl. Chem.* 291: 83–88.

Cao, J.J., Chow, J.C., Tao, J., Lee, S.C., Watson, J.G., Ho, K.F., Wang, G.H., Zhu, C.S. and Han, Y.M. (2011). Stable carbon isotopes in aerosols from Chinese cities: influence of fossil fuels. *Atmos. Environ.* 45: 1359–1363.

Chen, L.W.A., Lowenthal, D.H., Watson, J.G., Koracin, D., Kumar, N., Knipping, E.M., Wheeler, N., Craig, K. and Reid, S. (2010). Toward effective source apportionment using positive matrix factorization: Experiments with simulated PM$_{2.5}$ data. *J. Air Waste Manage. Assoc.* 60: 43–54.

Chen, Y., Cao, J.J., Zhao, J., Xu, H.M., Arimoto, R., Wang, G.H., Han, Y.M., Shen, Z.X. and Li, G.H. (2014). N-alkanes and polycyclic aromatic hydrocarbons in total suspended particulates from the southeastern Tibetan Plateau: Concentrations, seasonal variations, and sources. *Sci. Total Environ.* 470–471: 9–18.

Chow, J.C., Watson, J.G., Lu, Z., Lowenthal, D.H., Frazier, C.A., Solomon, P.A., Thuillier, R.H. and Magliano, K. (1996). Descriptive analysis of PM$_{2.5}$ and PM$_{10}$ at regionally representative locations during SJVAQS/AUSPEX. *Atmos. Environ.* 30: 2079–2112.

Contini, D., Genga, A., Cesari, D., Siciliano, M., Donateo, A., Bove, M.C. and Guascito, M.R. (2010). Characterization and source apportionment of PM$_{10}$ in an urban background site in Lecce. *Atmos. Res.* 95: 40–54.

Dai, Q.L., Bi, X.H., Liu, B.S., Li, L.W., Ding, J., Song, W.B., Bi, S.Y., Schulze, B.C., Song, C.B., Wu, J.H., Zhang, Y.F., Feng, Y.C. and Hopke, P.K. (2018). Chemical nature of PM$_{2.5}$ and PM$_{10}$ in Xi'an, China: Insights into primary emissions and secondary particle formation. *Environ. Pollut.* 240: 155–166.

Deng, J.J., Zhang Y.R., Qiu, Y.Q., Zhang, H.L., Du, W.J., Xu, L.L., Hong, Y.W., Chen, Y.T. and Chen, J.S. (2018). Source apportionment of PM$_{2.5}$ at the Lin'an regional background site in China with three receptor models. *Atmos. Res.* 202: 23–32.

Fang, X., Bi, X., Xu, H., Wu, J., Zhang, Y. and Feng, Y. (2017). Source apportionment of ambient PM$_{10}$, and PM$_{2.5}$ in Haikou, China. *Atmos. Res.* 190: 1–9.

Gao, X.M., Yang, L.X., Cheng, S.H., Gao, R., Zhou, Y., Xue, L.K., Shou, Y.P., Wang, J., Wang, X.F., Nie, W., Xu, P. and Wang, W.X. (2011). Semi-continuous measurement of water-soluble ions in PM$_{2.5}$ in Jinan, China: Temporal variations and source apportionments. *Atmos. Environ.* 45: 6048–6056.

Gu, J.X. Bai, Z.P., Liu, A.X., Wu, L.P., Xie, Y.Y., Li, W.F., Dong, H.Y. and Zhang, X. (2010). Characterization of atmospheric organic carbon and element carbon of PM$_{2.5}$ and PM$_{10}$ at Tianjin, China. *Aerosol Air Qual. Res.* 10: 167–176.

Gu, J.X., Bai, Z.P., Li, W.F., Wu, L.P., Liu, A.X., Dong, H.Y. and Xie, Y.Y. (2011). Chemical composition of

PM$_{2.5}$ during winter in Tianjin, China. *Particuology* 9: 215–221.

Gu, J.X., Du, S.Y., Han, D.W., Hou, L.J., Yi, J., Xu, J., Liu, G.H., Han, B., Yang, G.W. and Bai, Z.P. (2014). Major chemical compositions, possible sources, and mass closure analysis of PM$_{2.5}$ in Jinan, China. *Air Qual. Atmos. Health* 7: 251–262.

He, Q.S., Yan, Y.L., Guo, L.L., Zhang, Y.L., Zhang, G.X. and Wang, X.M. (2017). Characterization and source analysis of water-soluble inorganic ionic species in PM$_{2.5}$ in Taiyuan city, China. *Atmos. Res.* 184: 48–55.

Heo, J.B., Hopke, P. and Yi, S.M. (2009). Source apportionment of PM$_{2.5}$ in Seoul, Korea. *Atmos. Chem. Phys.* 9: 4957–4971.

Hleis, D., Fernandez-Olmo, I., Ledoux, F., Kfoury, A., Courcot, L., Desmonts, T. and Courcot, D. (2013). Chemical profile identification of fugitive and confined particle emissions from an integrated iron and steel making plant. *J. Hazard. Mater.* 250–251: 246–255.

Huang, L.K. and Wang, G.Z. (2014). Chemical characteristics and source apportionment of atmospheric particles during heating period in Harbin, China. *Acta Sci. Circumst.* 26: 2475–2483. (in Chinese)

Khan, M.F., Latif, M.T., Lim, C.H., Amil, N., Jaafar, S.A., Dominick, D., Nadzir, M.S.M, Sahani, M. and Tahir, N.M. (2015). Seasonal effect and source apportionment of polycyclic aromatic hydrocarbons in PM$_{2.5}$. *Atmos. Environ.* 106: 178–190.

Lan, Y., Yang, L.X., Yuan, Q., Yan, C., Dong, C., Meng, C.P., Sui, X., Yang, F., Lu, Y.L. and Wang, W.X. (2016). Sources apportionment of PM$_{2.5}$ in a background site in the North China Plain. *Sci. Total Environ.* 541: 590–598.

Li, M.H., Fan, L.C., Mao, B., Yang, J.W., Choi, A.M.K., Cao, W.J. and Xu, J.F. (2016). Short-term exposure to ambient fine particulate matter increases hospitalizations and mortality in COPD: A systematic review and meta-analysis. *Chest* 149: 447–458.

Lin, Y.C., Tsai, C.J., Wu, Y.C., Zhang, R., Chi, K.H., Huang, Y.T., Lin, S.H. and Hsu, S.C. (2015). Characteristics of trace metals in traffic-derived particles in Hsuehshan Tunnel, Taiwan: Size distribution, potential source, and finger printing metal ratio. *Atmos. Chem. Phys.* 15: 4117–4130.

Liu, B.S., Song, Na., Dai, Q.L., Mei, R.B., Sui, B.H., Bi, X.H. and Feng. Y.C. (2016a). Chemical composition and source apportionment of ambient PM$_{2.5}$ during the non-heating period in Taian, China. *Atmos. Res.* 170: 23–33.

Liu, B.S., Liang, D.N., Yang, J.M., Dai, Q.L., Bi, X.H., Feng, Y.C., Yuan, J., Xiao, Z.M., Zhang, Y.F. and Xu, H. (2016b). Characterization and source apportionment of volatile organic compounds based on 1-year of observational data in Tianjin, China. *Environ. Pollut.* 218: 757–769.

Liu, B.S., Bi, X.H., Feng, Y.C., Dai, Q.L., Xiao, Z.M., Li, L.W., Wu, J.H., Yuan, J. and Zhang Y.F. (2016c). Fine carbonaceous aerosol characteristics at a megacity during the Chinese Spring Festival as given by OC/EC online measurements. *Atmos. Res.* 181: 20–28.

Liu, B.S., Wu, J.H., Zhang, J.Y., Wang, L., Yang, J.M., Liang, D.N., Dai, Q.L., Bi, X.H., Feng, Y.C., Zhang, Y.F. and Zhang, Q.X. (2017a). Characterization and source

apportionment of PM$_{2.5}$, based on error estimation from EPA PMF 5.0 model at a medium city in China. *Environ. Pollut.* 222: 10–22.

Liu, B.S., Yang, J.M., Yuan, J., Wang, J., Dai, Q.L, Li, T.K., Bi, X.H., Feng, Y.C. Xiao, Z.M., Zhang, Y.F. and Xu, H. (2017b). Source apportionment of atmospheric pollutants based on the online data by using PMF and ME2 models at a megacity, China. *Atmos. Res.* 185: 22–31.

Liu, B.S., Cheng, Y., Zhou, M., Liang, D.N., Dai, Q.L., Wang, L., Jin, W., Zhang, L.Z., Ren, Y.B., Zhou, J.B., Dai, C.L., Xu, J., Wang, J., Feng, Y.C. and Zhang, Y.F. (2018). Effectiveness evaluation of temporary emission control action in 2016 in winter in Shijiazhuang, China. *Atmos. Chem. Phys.* 18: 7019–7039.

Liu, X.G., Li, J., Qu, Y., Han, T., Hou, L., Gu, J., Chen, C., Yang, Y., Liu, X., Yang, T., Zhang, Y., Tian, H. and Hu, M. (2013). Formation and evolution mechanism of regional haze: A case study in the megacity Beijing, China. *Atmos. Chem. Phys.* 13: 4501–4514.

Ma, Z.Z., Li, Z., Jiang, J.K., Ye, Z.X., Deng, J.G. and Duan, L. (2015). Characteristics of water-soluble inorganic ions in PM$_{2.5}$ emitted from coal fired power plants. *Environ. Sci.* 36: 2361–2366. (in Chinese)

Mohammed, G., Karani, G. and Mitchell, D. (2017). Trace Elemental Composition in PM$_{10}$ and PM$_{2.5}$ Collected in Cardiff, Wales. *Energy Procedia* 111: 540–547.

Murillo, J.H., Ramos, A.C., García, F.Á., Jiménez, S.B., Cárdenas, B. and Mizohata, A. (2012). Chemical composition of PM$_{2.5}$, particles in Salamanca, Guanajuato Mexico: Source apportionment with receptor models. *Atmos. Res.* 107: 31–41.

Okuda, T., Okamoto, K., Tanaka, S., Shen, Z.X., Han, Y.M. and Huo, Z.Q. (2010). Measurement and source identification of polycyclic aromatic hydrocarbons (PAHs) in the aerosol in Xi'an, China, by using automated column chromatography and applying positive matrix factorization (PMF). *Sci. Total Environ.* 408: 1909–1914.

Paatero, P. and Tapper, U. (1994). Positive matrix factorization: A non-negative factor model with optimal utilization of error estimates of data values. *Environmetrics* 5: 111–126.

Paatero, P., Eberly, S., Brown, S.G. and Norris, G.A. (2014). Methods for estimating uncertainty in factor analytic solutions. *Atmos. Meas. Tech.* 7: 781–797.

Peng, X., Shi, G.L., Liu, G.R., Xu, J., Tian, Y.Z., Zhang, Y.F., Feng, Y.C. and Russell, A.G. (2017). Source apportionment and heavy metal health risk (HMHR) quantification from sources in a southern city in China, using an ME2-HMHR model. *Environ. Pollut.* 221: 335–342.

Qiu, X.H., Duan, L., Gao, J., Wang, S.L., Chai, F.H., Hu, J., Zhang, J.C. and Yun, Y.R. (2016). Chemical composition and source apportionment of PM$_{10}$ and PM$_{2.5}$ in different functional areas of Lanzhou. *J. Environ. Sci.* 40: 75–83.

Rogula-Kozłowska, W., Błaszczak, B., Szopa, S., Klejnowski, K., Sówka, I., Zwoździak, A., Jabłońska, M. and Mathews, B. (2012). PM$_{2.5}$ in the central part of Upper Silesia, Poland: Concentrations, elemental composition, and mobility of components. *Environ. Monit. Assess.* 185: 581–601.

Russell, A.G., McRae, G.J. and Cass, G.R. (1983).

Mathematical modeling of the formation and transport of ammonium nitrate aerosol. *Atmos. Environ.* 17: 949–964.

Schauer, J.J., Kleeman, M.J., Cass, G.R. and Simoneit, B.R.T. (2002). Measurement of emissions from air pollution sources. 5. C-1-C-32 organic compounds from gasoline powered motor vehicles. *Environ. Sci. Technol.* 36: 1169–1180.

Schleicher, N.J., Norra, S., Chai, F., Chen, Y., Wang, S., Cen, K., Yu, Y. and Stueben, D. (2011). Temporal variability of trace metal mobility of urban particulate matter from Beijing – A contribution to health impact assessments of aerosols. *Atmos. Environ.* 45: 7248–7265.

SEPA (1990). Background Contents on Elements of Soils in China (in Chinese).

Shafer, M.M., Toner, B.M., Overdier, J.T., Schauer, J.J., Fakra, S.C., Hu, S., Herner, J.D. and Ayala, A. (2012). Chemical speciation of vanadium in particulate matter emitted from diesel vehicles and urban atmospheric aerosols. *Environ. Sci. Technol.* 46: 189–195.

Shakya, K.M., Peltier, R.E., Shrestha, H. and Byanju, R.M. (2017). Measurements of TSP, PM_{10}, $PM_{2.5}$, BC, and PM chemical composition from an urban residential location in Nepal. *Atmos. Pollut. Res.* 8: 1123–1131.

Tao, J., Cheng, T.T., Zhang, R.J., Cao, J.J., Zhu, L.H., Wang, Q.Y., Luo, L. and Zhang, L.M. (2013). Chemical composition of $PM_{2.5}$ at an urban site of Chengdu in southwestern China. *Adv. Atmos. Sci.* 30: 1070–1084.

Tao, J., Gao, J., Zhang, L., Zhang, R., Che, H., Zhang, Z., Lin, Z., Jing, J., Cao, J. and Hsu, S.C. (2014). $PM_{2.5}$ pollution in a megacity of southwest China: source apportionment and implication. *Atmos. Chem. Phys.* 14: 8679–8699.

Tian, Y.Z., Liu, J.Y., Han, S.Q., Shi, X.R., Shi, G.L., Xu, H., Yu, H.F., Zhang, Y.F., Feng, Y.C. and Russell, A.G. (2018). Spatial, seasonal and diurnal patterns in physicochemical characteristics and sources of $PM_{2.5}$ in both inland and coastal regions within a megacity in China. *J. Hazard. Mater.* 342: 139–149.

Truex, T.J., Pierson, W.R. and Mckee, D.E. (1980). Sulfate in diesel exhaust. *Environ. Sci. Technol.* 14: 1118–1121.

Tullio, A.D., Reale, S., Ciammola, M., Arrizza, L., Picozzi, P. and De Angelis, F. (2008). Characterization of atmospheric particulate: relationship between chemical composition, size and emission source. *Chemsuschem* 1: 110–117.

Turpin, B.J. and Huntzicker, J.J. (1991). Secondary formation of organic aerosol in the Los Angeles Basin: A descriptive analysis of organic and elemental carbon concentrations. *Atmos. Environ.* 25: 207–215.

Wang, P., Cao, J.J., Shen, Z.X., Han, Y.M., Lee, S.C., Huang, Y., Zhu, C.S., Wang, Q.Y., Xu, H.M. and Huang, R.J. (2015). Spatial and seasonal variations of $PM_{2.5}$ mass and species during 2010 in Xi'an, China. *Sci. Total Environ.* 508: 477–487.

Wang, Y., Zhuang, G., Tang, A., Yuan, H., Sun, Y., Chen, S. and Zheng, A. (2005). The ion chemistry and the source of $PM_{2.5}$ aerosol in Beijing. *Atmos. Environ.* 39: 3771–3784.

Wang, Y., Zhuang, G.S., Sun, Y.L. and An, Z.S. (2006). The variation of characteristics and formation mechanisms of aerosols in dust, haze, and clear days in Beijing. *Atmos.*

Environ. 40: 6579–6591.

Watson, J.G., Chow, J.C. and Houck, J.E. (2001). $PM_{2.5}$ chemical source profiles for vehicle exhaust, vegetative burning, geological material, and coal burning in Northwestern Colorado during 1995. *Chemosphere* 43: 1141–1151.

World Health Organization (2006). WHO air quality guidelines for particulate matter, ozone, nitrogen dioxide and sulfur dioxide: Global update 2005, Summary of risk assessment. World Health Organization, Geneva.

Wu, H., Zhang, Y.F., Han, S.Q., Wu, J.H., Bi, X.H., Shi, G.L., Wang, J., Cai, Z.Y., Liu, J.L. and Feng, Y.C. (2015). Vertical characteristics of $PM_{2.5}$ during the heating season in Tianjin, China. *Sci. Total Environ.* 523: 152–160.

Xu, H.M., Cao, J.J., Ho, K.F., Ding, H., Han, Y.M., Wang, G.H., Chow, J.C., Watson, J.G., Khol, S.D., Qiang, J. and Li, W.T. (2012). Lead concentrations in fine particulate matter after the phasing out of leaded gasoline in Xi'an. China. *Atmos. Environ.* 46: 217–224.

Xu, L.L., Yu, Y.K., Yu, J.S., Chen, J.S., Niu, Z.C., Yin, L.Q., Zhang, F.W., Liao, X. and Chen, Y.T. (2013). Spatial distribution and sources identification of elements in $PM_{2.5}$ among the coastal city group in the Western Taiwan Strait region, China. *Sci. Total Environ.* 442: 77–85.

Yan, D., Lei, Y.L., Shi, Y.K., Zhu, Q., Li, L. and Zhang, Z.E. (2018). Evolution of the spatiotemporal pattern of $PM_{2.5}$ concentrations in China – A case study from the Beijing-Tianjin-Hebei region. *Atmos. Environ.* 183: 225–233.

Yang, F., Tan, J., Zhao, Q., Du, Z., He, K., Ma, Y., Duan, F., Chen, G. and Zhao, Q. (2011). Characteristics of $PM_{2.5}$ speciation in representative megacities and across China. *Atmos. Chem. Phys.* 11: 5207–5219.

Yang, H.N., Chen, J., Wen, J.J., Tian, H.Z. and Liu, X.G. (2016). Composition and sources of $PM_{2.5}$ around the heating periods of 2013 and 2014 in Beijing: implications for efficient mitigation measures. *Atmos. Environ.* 124: 378–386.

Yu, L., Wang, G., Zhu, G. and Zhang, R. (2010). Characteristics and sources of elements in atmospheric particles before and during the 2008 heating period in Beijing. *Acta Sci. Circumst.* 30: 204–210. (in Chinese)

Zhang, F., Wang, Z.W., Cheng, H.R., Lv, X.P., Gong, W., Wang, X.M. and Zhang, G. (2015). Seasonal variations and chemical characteristics of $PM_{2.5}$ in Wuhan, central China. *Sci. Total Environ.* 518–519: 97–105.

Zhang, F.W., Xu, L.L., Chen, J.S., Chen, X.C. and Niu, Z.C. (2013). Chemical characteristics of $PM_{2.5}$ during haze episodes in the urban of Fuzhou, China. *Particuology* 11: 264–272.

Zhang, L.L., Gao, Y.X., Dao, X., Wang, C. and Teng, E.J. (2014). Composition and distribution of elements in air particulate matters during heating season of Beijing-Tianjin-Hebei Megacities, China. *Environ. Monit. China* 30: 53–61. (in Chinese)

Zhang, R., Shen, Z., Cheng, T., Zhang, M. and Liu, Y. (2010). The elemental composition of atmospheric particles at Beijing during Asian dust events in spring 2004.

Aerosol Air Qual. Res. 10: 67–75.

Zhang, Y., Shao, M., Zhang, Y.H., Zeng, L.M., He, L.Y., Zhu, B., Wei, Y.I. and Zhu, X.L. (2007). Source profiles of particulate organic matters emitted from cereal straw burning. *J. Environ. Sci.* 19: 167–175.

Zhang, Y.F., Xu, H., Tian, Y.Z., Shi, G.L., Zeng, F., Wu, J.H., Zhang, X.Y., Li, X., Zhu, T. and Feng, Y.C. (2011). The study on vertical variability of PM and the possible sources on a 220 m tower, in Tianjin, China. *Atmos. Environ.* 45: 6133–6140.

Zhang, Y.J., Cai, J., Wang S.X., He, K.B. and Zheng, M. (2017). Review of receptor-based source apportionment research of fine particulate matter and its challenges in China. *Sci. Total Environ.* 586: 917–929.

Zhou, M., Qiao, L., Zhu, S., Li, L., Lou, S., Wang, H., Wang, Q., Tao, S., Huang, C. and Chen C. (2016). Chemical characteristics of fine particles and their impact on visibility impairment in Shanghai based on a 1-year period observation. *Acta Sci. Circumst.* 48: 151–160. (in Chinese)

Zhu, C.S., Cao, J.J., Shen, Z.X., Liu, S.X., Zhang, T., Zhao, Z.Z., Xu, H.M. and Zhang, E.K. (2012). Indoor and outdoor chemical components of $PM_{2.5}$ in the rural areas of Northwestern China. *Aerosol. Air Qual. Res.* 12: 1157–1165.